Rib Cage Segmentation in CT Scans

Literature Review Biomedical Image Science

14 October 2013

Enrico Contini – 3913511

Supervisor: *Dr. Josien Pluim*
Daily Supervisor: *Yolanda Noorda*

Table of Contents

1. Introduction

The segmentation of the rib cage in CT images represents a task of primary importance in medical imaging for different reasons. First of all, ribs provide a convenient frame of reference in the chest and make it possible to localize organs such as heart, lungs and vertebral bodies, and also to accurately register intra or inter – patient scans. Secondly, from the study of the segmented bone itself several features can be extrapolated, that are indices of the presence of some diseases. For example, deformed or incompletely formed ribs may be the sign of rickets or neurofibromatosis. Moreover, dense or sclerotic ribs may also be a sign of cancer, as well as end-stage renal disease, or other metabolic diseases. Frequently for 3D visualization purposes, vertebrae and ribs need to be removed to allow a better view of the interested organs.
While the need for reliable segmentations of rib cages is emphasized by these applications, the task of rib cage segmentation is still an open challenge for a number of reasons: ribs may have no clear boundaries; some rib or parts of ribs may be missing, and scans obtained in clinical practice often contain pathologies like scoliosis, that cause complex deformations of the rib cage including rotation and distortions.
This literature study aims to give a critical review of the methods currently used for segmenting the rib cage. Each method is accurately analyzed, highlighting its strong and weak points in comparison with the other methods, indicating its suitability for clinical usage and possible improvements.

2. Literature examination

Given the importance of rib cage segmentation, the topic has been studied for several decades, and frequently on other imaging techniques like radiographs [21]-[24] or biplanar X-ray images [25]-[31]. The rib cage segmentation and 3D reconstruction from biplanar X-rays is having quite some interest in the research world since it does not expose the patient to a high radiation dose like CT and it gives results with an accuracy close to that of CT-scans reconstructions [15].
However, the methods investigated in this study were taken from fifteen research works on CT scans published from 1999 to 2013. They involved the segmentation of rib cages of healthy patients as well as of patients presenting pathologies or fractures [13] and pediatric patients [2]. The remainder of this paper describes the different methods, their abilities and weaknesses, their reliability and robustness, with a final in-depth discussion of the problems faced and the solutions that they proposed.

3. Methodologies Overview

Research on segmentation can be categorized into two main groups: methods that incorporate rib cage shape models or prior anatomical knowledge and those that do not use any kind of prior knowledge.
When using rib cage models, the purpose is to fit the model into the patient's rib cage image, allowing only some types of transformations and trying to reduce a distance function between the model rib cage and the imaged one. Those rib cage shape models derive usually from statistical shape model created from a dataset of other segmented rib cages. Instead, prior anatomical knowledge is employed for example when adding some constraint to the segmentation process or during the training phase of a classification algorithm, which requires a database of similar cases to learn how to classify the new images. While these approaches that exploit prior knowledge work well in many cases, they may fail to perform robustly for a data set containing a large variety of 3D image data, due to variation in bone appearance.
The other methods are rather different from each other, but they are gathered from the fact that they do not use pre-established rib cage model or knowledge, instead they base their segmentation only on the image features.

3.1. Prior knowledge independent segmentation methods

3.1.1. Thresholding

In 2010, Furuhashi et al. [8] developed a computer-aided diagnosis system that labeled ribs and thoracolumbar vertebrae automatically. A candidate bone was extracted from the input volume data of the CT image by applying multiple pixel thresholding to the CT data and then detecting the regions of connected voxels obtained at each threshold. The different thresholds were determined automatically by histogram analysis, which showed three or four prevalent gray level distributions, corresponding to air, soft tissue, enhanced vessels and bones. The regions of connected voxels were obtained using 3D connected component labeling for the distribution of enhanced vessels and bones since they overlapped partially. The various parts of the candidate bone were then classified as representing bone, calcified lesions, or enhanced vessels according to a linear discriminate analysis using the effective features of distribution of CT values, the gradient strengths of the voxel values, and the anatomical characteristics of each independently classified region. The vertebrae were separated from the ribs based on their distances from the center of the vertebral bodies on the axial CT projection image. The ribs were segmented by extracting the continuous components using 3D connected-component labeling, and the lowest pair of ribs was then identified as the 12th ribs. The method was finally tested with 23 cases (13 males and 10 females).

In 2010, Banik et al. [2] proposed a method to segment the whole rib cage in CT images of pediatric patients. Rib structure and the vertebral column were initialized using multilevel thresholding and the results were refined using morphological image processing techniques. In first place, the CT volume was processed to identify and remove peripheral artifacts, the skin, and the peripheral fat using a multilevel thresholding approach based on their typical HU. After further thresholding at 200 HU, the resulting binarized image was morphologically opened to disconnect the ribs from the vertebrae. In a third stage, based on

the peripheral fat boundary, they defined a central line on each axial slice along the sagittal plane that passed through the spine. Then a region was considered to be part of a rib if it fulfilled a series of constraints based on the Euclidian distance to the defined midline and to the peripheral fat boundary. Extra constraints on the geometry of the detected regions were also added. Afterwards, to improve the detected rib structures, skeletonization by morphological thinning followed by opening and fuzzy connectivity analysis were applied. Then, the unwanted structures detected inside elliptical region defined by the rib structures were eliminated. Finally, after removing the voxels corresponding to other regions and filling in holes, the resulting volume was dilated in 2D using a disk-type structuring element of radius 2 pixels, to obtain a refined result of segmentation of the rib structure.

In 2009, the work of Zhou et al. [4] used an automated scheme for segmenting the bone regions and recognizing the bone structure in non-contrast torso CT images. This scheme included two principal parts: bone region segmentation and bone structure recognition, see fig. 1. To segment the bone regions they used gray-level thresholding to keep the high generality. In order to achieve also high accuracy they used a new method to decide the optimum threshold value for each patient case specifically using a dynamic histogram analysis. This analysis assumed the bone region and liver region as Gaussian distributions and searched the best separation point (threshold value) of those two distributions by observing its variations. The bone regions were then divided and categorized into 60 categories such as vertebras (18), ribs (12), sternum (3) and so on. The bone regions were modeled as a connection of 60 components firstly, and then a coarse-to-fine, global-to-local bone region splitting was proceeded with the use of implicit anatomical knowledge to accomplish the bone structure recognition. Although, the authors claimed that the algorithm was fully automatic, they did not present any detailed description of the segmentation step.

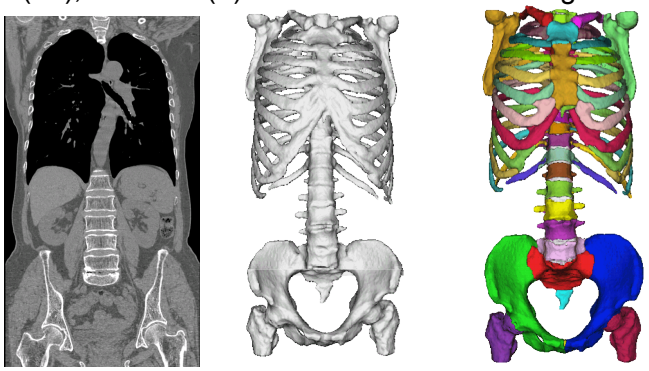

Fig. 1: Outline of the scheme for bone structure recognition.

3.1.1. Recursive tracing

In 2004, Shen et al. [3] proposed a segmentation algorithm for the extraction and labeling of individual rib structures based on a recursive tracing approach. To obtain one seed point for each rib, they first selected a coronal plane close to the center of the chest. This plane made intersections with all the ribs, but did not contain any point from the spine or sternum. On this coronal image, the intersections of the ribs were small ellipses lining up uniformly around the border of the lungs. A bone threshold (undeclared value) was then applied to binarize the image, size constraints were applied to rule out most of the false regions, and the centroids of the remaining regions were recorded as seed candidates. The contours of the lung boundaries were also extracted. Valid seed candidates were required to be close enough to the outer lung boundary, and uniformly distributed along the boundary. Starting at each seed point, they traced in both directions, and merged the two partial tracing results. The smallest eigenvector of the covariance matrix of the rib cross-section was taken as the centerline direction of the detected seed point. This eigenvector should point indeed in the direction perpendicular to the rib cross-section, since it is the eigenvector associated with the smallest eigenvalue, so with the smallest variance. Once the seed points for every ribs had been found, they searched the edges of the ribs sections by selecting those edges that have high

enough gradient magnitudes and with their gradient directions pointing out of the outer surface. To obtain the best contour, they used dynamic programming, estimating the best rib edge on each direction for every cross-section. Once estimated the center point of the rib section from the obtained rib contours, they applied some rule to improve the accuracy on the tracing: the current tracing direction had to be close enough to the tracing directions of the previous 10 steps, and in the paths from the initial center point to the rib edges there should have been mostly high intensity voxels. However, if one of those conditions were not met the tracing process was not immediately terminated. Instead, the algorithm retrospectively made adjustment of the initial center location, allowing it to move in the close neighborhood, and the initial tracing direction could be adjusted by adding small deviations. For each of these adjustments, they carried the tracing procedure once more to see if the stopping criterions were met. If also the retrospective test failed, then the trace would have been terminated from the algorithm.

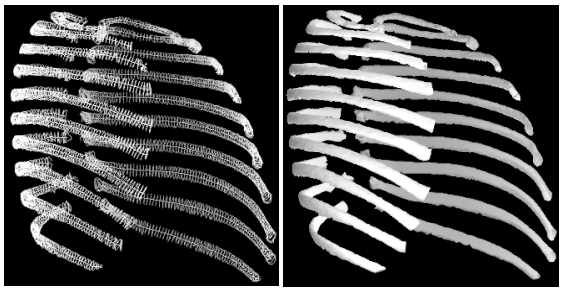

Fig. 2: An example result. (a) Extracted centerlines and contours that reflect the local shape. (b) Shaded surface display of the outer surface constructed from contours.

In 2010, H. Li et al. [10] presented a new method for automatic rib positioning and extraction in CT images. They used the Hough transform to find the first rib in a series of sagittal planes, looking for a line with a certain inclination angle and length. The geometrical constraints were indeed fixed for a length of at least 40mm, and an angle between 15 and 60 degrees. The plane in which the first rib was found was stored as Key Sagittal Plane (KSP). On this plane they extracted the rib contours and took the central points as the initial seed point. When the initial seed point of each rib was defined, they used a tracing based segmentation method as Shen et al. [3] to obtain the whole rib and give each rib the exact position label.

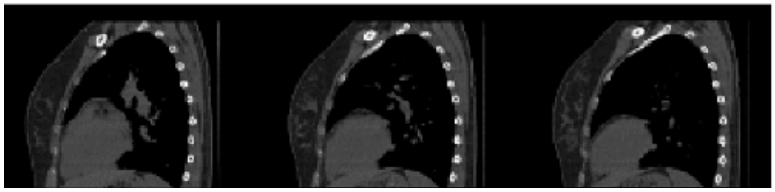

Fig. 3: Feature of the first rib on sagittal plane (moving from subcentral of the body to the left or right side

In 2012, Zhang et al. [12] developed an algorithm that attained the complete and isolated segmentation of 12 pair of ribs with a recursive tracking on coronal slices spreading from the middle coronal slice. As Shen et al. [3] previously did, at each coronal slice the lung contours were found by thresholding at -500HU and applying a gradient magnitude filter. Candidate ribs regions were also derived from thresholding with a value of 110HU, then most of the non-rib regions were eliminated by employing constraints on shape, size and location with respect to lung contours. Appropriate thresholds are chosen so that the cartilage is binarized as background to break the connection between the sternum and the ribs. Then the center points of the rib regions were saved as the centroid points for the following tracking procedure. Starting from the centroid points the tracking process is initiated in both direction, toward the sternum and toward the spinal column. At each coronal slice rib regions were searched in the binarized image around the corresponding centroid point within a radius of 50pixels. After all rib regions were found, the centroid point was updated for processing the next slice. When going toward the spine they included an

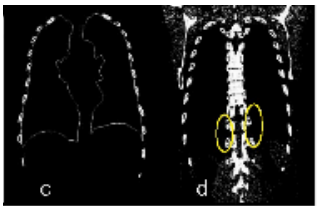

Fig. 4: 355th coronal slice in which rib regions appear between the left and right lungs boundaries

additional step in which they searched for rib regions also around the contour of the middle boundary of the lungs and vertically 100 pixel below the most inferior pair of ribs. This extra step was necessary both to prevent missing rib regions which are between the right and left lung contours when images contain spine regions and also to find new rib regions i.e. the 10th, 11th, 12th pairs of ribs. Since the segmentation algorithm developed by the group of Zhang was meant to deal with isotropic data, they resampled the CT data and also used a median filter for noise removal in a preprocessing step.

In 2012, Yao et al. [14] developed a rib segmentation method included in a Computed Aided Detection (CAD) system, with the purpose of supporting radiologists in the process of finding sclerotic bone metastasis in ribs in CT images. The method started with the segmentation of the spine. Employing an algorithm previously developed from the same group [16], that used thresholding, region growing and vertebra template matching, the spine was segmented to allow the localization of the ribs. Subsequently, the ribs were segmented in three steps. The bony structures with an intensity value greater than 200HU and within 2cm from the segmented spine were detected. Then, a cross section was defined at the centroid of each detected structure, see fig.5. These cross section were determined by minimizing the bony area present in the cross-section itself. After the first cross sections had been found, the algorithm fitted a B-spline curve through the center points to determine the current centerline. The tangent to the B-spline curve at the center point of one cross section represented the normal vector of the next cross section, defined at a precise step-size along this normal. The step-size was set as the inplane pixel size of the CT slice. The pixel values on the cross section were obtained by trilinear interpolation from the original 3D CT image. Afterwards, the centerline location was defined by maximizing the overlap of the bone pixels between the two consecutive cross sections, and minimizing the distance between their center points. In the last stage, rib centerlines that were shorter than a preestablished threshold were eliminated. Moreover, if more than one rib per vertebra was detected, the shorter one was eliminated. The rib segmentation was achieved by stacking all the cross sections and back-projecting to the original CT data.

Fig.5: Cross section initialization

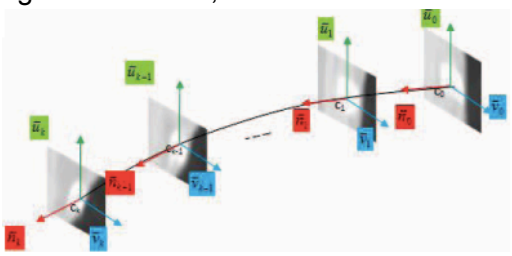

Fig. 6: Rib centerline progressive tracing

3.1.1. Region growing

In 1999, Fiebich et al. [7] presented a new segmentation method for bony structure in CT scans. Their method was based on an automatic iterative region growing technique. The seeds for growing the 3D volumes were selected among those voxels with a gray value that exceeded an establish threshold, see table 1. The volumes were grown using a second specified threshold in the full data set (1st iteration). To eliminate calcifications and other nonbone structures the regions with a volume smaller than 5 cm^3 were discarded. The remaining regions were then used as seeds for a second volume growing with using a third specified threshold and intervoxel gradients. The different threshold and gradient parameters for each body part were evaluated empirically from three CT data set. The first iteration, produced an incoplete segmentation of the bone structures. Therefore, the second iteration used a lower threshold to achieve the complete segmentation of the bone, in combination

with gradient threshold, preserving in this way also the boundaries of the structures. The segmentation process was then concluded by a dilation operation, to include also on the periphery of bony structures. This segmentation technique was tested on 40 CT images, of which 10 were chest-CT.

Examination type	Initial threshold	Second threshold (in first iteration)	Third threshold (in second iteration)	Maximum gradient
CT skull	750 HU	400 HU	180 HU	25 HU
CT chest	400 HU	190 HU	130 HU	100 HU
CT abdomen	460 HU	340 HU	150 HU	25 HU

Table 1 : Threshold and maximum gradient values used in segmentation of bony structures for different examination types

In 2002, Kim et al. [8] proposed a method to segment object in 3D image slices by tracking not only the target object but also its adjacent objects. This method was a hybrid technique including recursive tracing and region growing techniques. It was composed of three modules: segmentation, cartilage recovery and object tracking. In the first module the target object grown from initial user given seed points to regions with homogeneous gray value. The number of initial seed points was not specified by the authors. This module could detect/prevent a leakage given the image characteristics of the tracking objects. A leakage was detected when a non-target object was merged to a target object in the next slice. If a leakage was detected the two objects were separated with a minimum cost path finding function. The second module was the cartilage detection and recovering. To determine if a cartilage area existed in an image slice, a size change of the vertebrae segmentation results between two consecutive image slices was examined. For example, if the current slice had relatively smaller size of a vertebra than the one in the previous slice, a cartilage area was assumed to exist in the current slice. Next a cartilage area was recovered with a shape model of the vertebrae generated from the previous slice and gray value pixels in the current slice. The object tracking module propagated the segmentation results of a slice into the next slice, and the target object areas became the seeds for the region growing process in the next slice. This module generated also an alarm area by dilating the target object's boundaries to monitor adjacent non-target objects with similar gray value to see if they approached the target object. Ribs segmentation was performed with object propagation. Although ribs are connected to the vertebrae, ribs in image slices are either connected or disconnected to the vertebrae depending upon a viewing scope in image acquisition. The connected ribs could be segmented with propagation of the target objects, but on the other hand the disconnected ribs needed to receive seed points to start the region growing process.

Fig.7: Example of leakage detection

In 2010, Lee et al. [1] presented a fully automatic algorithm to segment the individual ribs from low-dose chest CT scans. The method consisted of the following four stages. First, the image was filtered with a 3x3 mean filter to reduce the noise. Then all the high-intensity bone structures present in the scan were segmented by thresholding at 175 HU. Any connected component that was smaller than 4500mm^3 in volume was considered as noise and was removed from the segmentation. The intensity and volume thresholds were empirically chosen from experimenting with 5 cases. In the second step, the centerline of the spinal canal was identified using a distance transform of the segmented bone. The starting seed point was automatically identified from the lowest 25mm of image slices, as an average of the centers of the spinal canal, local maxima in the distance transform image. Then, the entire canal was traced upward using an iterative algorithm starting at the seed point. In the third step, a seed region for each rib was identified by screening the segmented image region at a predefined distance (enough to not contain any vertebrae part) to the left and to the right of the spinal canal's centerline, see fig. 8. Within each plane, any voxel that belonged to a segmented bone was found, and a 3D connected component was grown within the plane starting at that voxel. Two criteria were used to determine if a detected seed

region actually belonged to a rib. First, its volume had to be greater than a pre-established threshold, and second, the component had to span through the entire width of bounded plane. Finally every detected seed region was grown into full rib and given a unique label. The outer portion of the rib was segmented using 3D region growing, by iteratively adding any connected voxels. When growing the rib outward, 8-connectivity was used in the 3D image space. To trace the inner portion of the rib a hollow cylindrical volume was fitted along the rib and iteratively advanced until it reaches the expected length of the inner rib portion. Each iteration determined the direction of the cylinder by finding the highest correlation to the pre-filtered CT image. The expected length of the interior part of the ribs was determined by taking the distance between the seed region and the center of spinal canal.

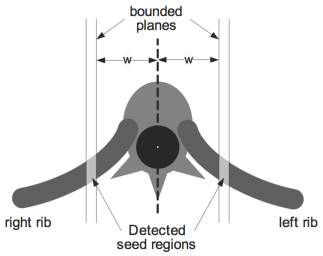

Fig. 8: Seed detection method

Recently in 2012, Ramakrishnan et al. [13] developed a complete automatic system to extract 3D centerlines of the ribs from thoracic CT scans, that could form the basis for a further segmentation of the ribs. The method was divided in the following three parts. a) Pre-trace processing: in axial slices spaced 10mm, the volume of interest including the rib cage was modeled in terms of connected components of voxels with intensities higher than 175HU. They used the location of the spinal canal centerline in order to guide the rib tracing in the vicinity of the spine and also to determine where to stop the rib trace. The spinal canal was fully detected in the axial images by morphological processing followed by finding the best fit for a ring shape object. Then using Kalman filtering the spinal canal was tracked through consecutive 2D spine cross-sections in order to trace the spine centerline. For detecting the rib seed points, three centrally located coronal planes and twelve evenly spaced sagittal slices within the thoracic cage's anatomy were chosen. Here, the bone regions were found through connected component analysis and the centroids of those connected component regions that met rib size constraints were considered to be potential rib seed points. The next step was the 3D rib orientation determination: they considered all voxels with intensity higher than 75HU within a small subvolume of 20mm x 20mm x 20mm around the rib seed point to be part of the rib bone, and determined the rib orientation as the optimal direction that was simultaneously orthogonal to the image gradients and parallel with the direction of the rib position of the bone voxels in that small subvolume, see fig. 10. b) The second stage involved the rib centerline tracing. Ramakrishnan's group used the Random Walker algorithm that extracted at each rib seed point a 2D cross-section of 27mm x 27mm orthogonal to seed point direction that contained fully the rib geometry without containing neighbor ribs. Then the algorithm estimated the rib center point from the extracted rib contours. Next, they used the Kalman filter to trace the rib centerline whose state space models the natural curvature of the rib centerline. The rib centerlines were traced progressively in both forward and backward directions from each seed point. c) The final stage was post-trace processing where the rib components distant less than 4.0mm were merged into complete ribs. In order to classify non-ribs from actual ribs a multilayer perception was employed to score the centerline based on a "ribness" score, composed of 34 features from spatial, shape and physical characteristics. Successively the ribs were

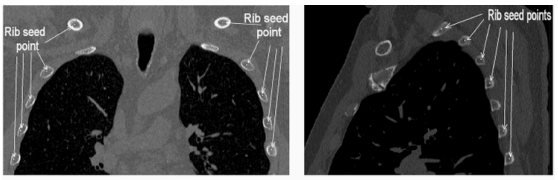

Fig. 9: Rib seed points in a) coronal and b) sagittal image

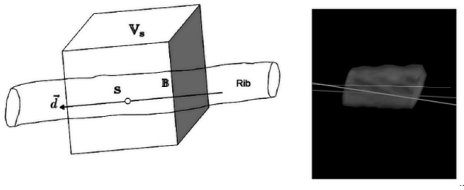

Fig. 10: Illustration of the 3D subvolume

placed in their correct axial order, paired and labeled by computing the centroids point of every centerline and evaluating their position with respect the spine centerline.

3.2. Prior knowledge based segmentation methods

3.2.1. Rib cage model based

In 2007, Klinder et al. [5] presented a new model-based approach for an automated labeling and segmentation of the rib cage in chest CT scans. Initially a triangulated surface model of all 24 ribs and all 24 presacral vertebrae was created. The vertebra model generation was based on the scanning of plastic phantoms, while the rib models were created from segmentation of patient CT data. Then the model was adapted to a sample of 29 CT data sets showing different portions of the rib cage and the vertebral column. To position correctly the created model to new CT scans they used a ray search based approach, as done also for segmentation on X-ray [20] and biplanar X-ray images. Rays pointing in head-foot direction and crossing a rib bone show a pattern of a high gray value when entering the rib through cortical bone followed by a lower one when traversing the bone marrow and again a high gray value exiting the rib through cortical bone, see fig. 11. If a ray owned the defined profile, the middle point of the two positions, where the ray enters and exits the rib, was saved as a rib candidate. Secondly, model centerlines and extracted centerlines were registered with an iterative closest point (ICP) algorithm allowing an affine transformation. The configuration with the minimal residual error was supposed to correspond to the true configuration. They also developed an alternative strategy for the positioning of the vertebrae model to overcome the problem of those CT scans that did not cover the entire chest. A local vertebral coordinate system (VCS) was defined from a cylinder fit to the vertebral foramen, the middle plane of the upper and lower vertebral body surfaces, and the vertebra's sagittal symmetry plane. By using the derived object relations expressed in the form of VCSs, the vertebra models could be iteratively positioned. Starting from one adapted vertebra model, neighboring models could be positioned in the data set by applying the transformation between corresponding vertebrae obtained from the vertebral column model.

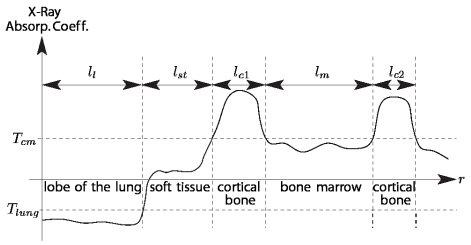

Fig. 11: Defined search profile for rib detection

In 2012, Wu et al. [11] proposed a new approach integrating rib seed point detection and template matching to detect and identify each rib in chest CT scans. In detail they developed a learning-based object specific centerline detection algorithm wherein the obtained probability map was used to track and label the rib centerlines. For the training stage 12 pairs of rib centerlines were manually annotated from 40 CT scans. 3D Haar-like features were selected due to their efficiency and to their effectiveness in object recognition. These features consider adjacent box regions at a specific location in a detection window, and calculate the difference between the sums of the pixel intensities within a region. Finally given a volume, the learned classifier Probabilistic Boosting Tree (PBT) would generate a probability response map that indicates the likelihood of each voxel of being a rib centerline. Since the obtained probability map was not always reliable for the presence of neighbor bone structure such as scapula or clavicle they introduced also a rib template

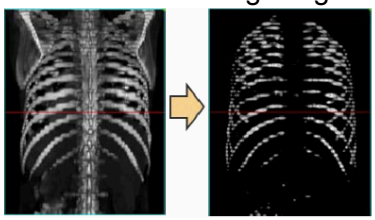
Fig. 12: Example of the rib centerline probability map

matching method. The intent of the method was to find the transformation that maximized the sum of response of the transformed template on the generated probability map. The new template matching method consisted of breaking each rib into several short segments, each one with a considerably lower degree of curvature of the entire rib. Therefore those rib segments could be approximately matched via rigid transformation by searching for the optimal similarity transform parameters. Each rib was split into 4 parts and starting from the segment connected to the central vertebrae, they searched for the optimal rigid transformation parameters. The result was used to initialize the pose of the next segment, and repeat the optimization, until all segments were matched. To avoid matching the segments to the wrong rib due to the similarity between adjacent ribs, they imposed a pairwise smoothness constraint on the transform parameters of neighboring rib segments. Finally, because each rib segment was transformed rigidly, the articulated rib centerline was piecewise smooth and subject to small deviation. So to further refine the matching results they employed an active contour model.

3.2.2. Prior knowledge based

Recently in 2013, Gargouri et al. [14] presented a paper in which they described an approach for the identification of the rib cage structures that leveraged the expertise of a user through a learning procedure. They proposed to use two new shape descriptors to be used in conjunction with a Random Forest (RF) classifier that enabled a reliable and robust identification of the ribcage structures. Each bone voxel was associated with a feature vector. The first shape descriptor they introduced was the Axial-inertia descriptor. In this descriptor they focused on the local geometry of each bone voxel B. In particular they proposed to evaluate the local curvature of the set of bone voxels in small sphere neighborhoods around the voxel B. The proposed feature vector was then composed by the biggest and the smallest eigenvalues for each neighborhood sphere. The neighborhood sphere varied from 10 to 30 voxels, giving so a feature vector with 42 elements. Since the magnitude of the maximum eigenvalue indicates how much aligned the bone voxels are, this descriptor was a measure of the deviation of the bone voxels from their principal direction, within neighborhood of increasing scale. The second descriptor was called Rotation Invariant Shape Context Descriptor. For each bone voxel B they computed 56 bands between spheres centered in B and of radius values randomly sampled between 2 and 35. Then for each band the number of bone voxels was calculated, yielding to a feature vector of dimension 56. Moreover, the two shape descriptors were evaluated in comparison with a simple intensity-based shape descriptor, in which for each voxel, 60 features were extracted from the average gray value of 60 random size boxes around that voxel. Finally, for each descriptor, the RF classifier was tested with 3,938 bone samples (48% rib-bones and 52% non rib-bones).

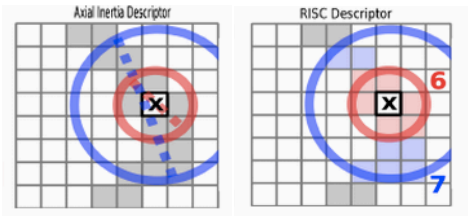

Fig. 13: Illustration of shape descriptors marked around a bone pixel B.

In 2007, Staal et al. [6] achieved the segmentation of the complete rib cage in CT images developing a method that used a general framework for automatic detection, recognition and segmentation of objects. The framework was composed of five main steps. (1) The image was binarized with a threshold at 100HU and then the 1D ridge voxels were detected. Since an elongated structure in a 3D image is a 1D curve, the tangential vector to this curve were determined by the eigenvector *V* of the Hessian matrix H with smallest eigenvalue in absolute value. A bright elongated structure has a maximum in the plane perpendicular to *V*

and so the detection of the 1D ridges was reduced to determine at every voxel whether there was a local maximum of the intensity in the normal plane. (2) The primitive elements were formed from the set of ridge voxels using a growing process that considered the local orientation of the ridge. The neighborhood around a ridge voxel was investigated and those ridge voxels that meet certain requirements on similarity of directions were added to the primitive. The seeds for this region growing process were chosen randomly from the available ridge voxels. (3) A Spin-glass classifier was used to distinguish ribs from other primitives. Two types of features have been used in this work: local features, including geometrical information of the primitives and intensity based information (total of 57 features), and features that encode a relationship between two primitives, including distance, mutual orientation and alignment measures (total of 15 features). After all features had been included, the subset that gives the best overall performance was chosen. For the feature selection process the training set was randomly split in 10 scans for training and 10 scans for evaluation. (4) In this stage the rib primitives were grouped into centerlines of the specific ribs by using the same constraints of step 2, but this time only with foreground primitives. The centerlines were further labeled to rib side and number by using two simple heuristic algorithms. (5) Finally for the full segmentation was employed a region growing algorithm. The algorithm included to the centerline all the neighboring voxels (within a radius of 40 voxels) with a gray value close to the average gray level of the centerline, updated iteratively.

4. Performances assessment

The issue of rib cage segmentation in medical images has been studied and approached in different ways by several research groups. Although the problem was already addressed in 1983 by Souza et al. [20] when investigating for an accurate detection of ribs in X-rays, and from other groups in the following decades dealing with both X-rays or biplanar X-ray images [21]-[31], volumetric images as CT scans required new segmentation techniques capable to cope with three dimensional image data, segmenting ribs structure within a reasonable amount of time. Therefore, a comprehensive overview of methods currently used with CT images has been presented in this study. While the majority of the studies deal with the segmentation of the complete rib cage, some of them considered only the ribs centerline extraction [11],[13], since they can form a coordinate system of the thoracic cage for localizing organs and record pathology locations. Nevertheless, those methods could constitute a reliable base to achieve the segmentation of entire rib cage in a further step.

4.1. Prior knowledge independent segmentation methods

Thresholding

To face the problem of threshold value selection, Furuhashi et al. [8] developed a method for the automatic detection of the threshold value based on the histogram analysis. The main disadvantage of this method is that the contrast-enhanced vessels and calcified lesions can

also be extracted because CT values overlap with those of bone. Therefore, they used a linear discriminant classifier to distinguish bone from non-bone structures. However, they did not specify the number of features used, neither how they chose the thresholds for the features. In the third step, to separate the ribs from the vertebrae, they used the rib distances from the center of vertebral bodies. The authors did not specify which distances were used. If those distances were pre-established using anatomical knowledge, they would probably be inaccurate when used with pediatric CT images or with different rib cage sizes, because the distances between ribs and vertebra centers are considerably shorter in children than in adults. Indeed, even if the patients presented quite different diseases (see table 2), constituting an ideal database for testing the algorithm, the ages ranged from 52–85 years old, so no young patient was included in this study. The work presented an evaluation of the automatic labeling part from one physician, which established that 27 of 42 scanned first ribs (64%) and 1 of 46 second ribs (2%) were mislabeled. However, the method needs to be further evaluated, since without a quantitative assessment of the segmentation results, it is difficult to predict its performance in a clinical setting.

Factors	($n = 23$)
Sex (M/F)	13/10
Age (years)	67.5 ± 11.0
Indications for CT	
Lung/mediastinal neoplasm	11
Chest abnormal shadow	4
Aortic lesion	4
Obstructive lung disease	2
Pulmonary embolism	2
Bone degenerations or complications	
Spondylosis	23
Osteoporosis	10
Scoliosis	1
Compression fracture	1
Contrast enhancement	
Dynamic	6
Enhancement	7
None	10

Table 2: Patient profiles

Also Zhou et al. [4] used dynamic histogram analysis to evaluate for each patient the best threshold value between the gray values of the liver and those of the bone structures. This can be a dangerous approach when the patient presents diseases that alter the typical gray value of the liver, as for example liver calcifications. The result in this case would be a shifted threshold value with the inclusion in the binarized image of unwanted structures, then classified and segmented as part of the bone regions from the algorithm. The present method was tested on a data set of 48 CT images (38 males; 10 females; ages: 20-88) with only one isotropic spatial resolution of about 0.63 mm, and no pediatric cases nor patients with diseases. In addition to liver disease, skeletal modifications could also cause issues, and as for pediatric patient scans, could lead to misclassifications during the bone structure recognition step. Therefore, the method is considered to be inclined to errors when used with clinical data. The group confirmed that the bone structure in 90% CT cases was successfully recognized based on a subjective validation of an anatomical expert. The successful ratios of vertebras, ribs, sternum and bones of upper limb recognitions were 92%, 98%, 90% and 96% respectively. Nevertheless, only the bones of the lower limb were quantitative evaluated, while an accuracy assessment of the rib cage is absent. Moreover the paper does not provide a thorough description of how the segmentation of the different bone structures was obtained, neither if the process was automatic or manual.

Instead, Banik et al. [2] used a fixed threshold of 200HU to binarize the image. The threshold value and few geometrical parameters were empirically determined from only a small subset of the CT images analyzed, avoiding in this way to overfit the algorithm to the training set characteristics. On the other hand, the effectiveness of the parameters is uncertain with other images, since the small size of the testing dataset does not permit assessment on the robustness of the method. Differently from Furuhashi [8], this study was based on both pediatric and adult patients, counting 39 CT exams of 13 subjects with age varying from 2 weeks to 20 years. Moreover, the CT exams had varying thickness resolution of 2.5 or 5 mm, and the in-plane resolution varied from 0.35 to 0.70 mm. In addition, their intuition of

considering the peripheral fat boundary to estimate the central line passing through the spine on the axial slices, made the algorithm totally independent of the position of the patient in the image. Exceptionally, in two cases, the patient being of age 2 weeks and 3 months respectively, a few parts of the rib structure were not detected because of the small size of the patient and the low spatial resolution of the image data. A limitation of the present work is that in all cases the results included the scapula, clavicles, and the humeri at the top of thoracic region. Therefore, to use this method for complete rib cage segmentation in clinical practice, further effort is required to eliminate undesired bone structures. These structures could be easily removed by using some kind of template matching technique for the rib cage, as for example Klinder [5]. Furthermore, while the results of the segmentation of vertebral column and spinal canal were assessed qualitatively and quantitatively the ribs' segmentation results were only qualitatively evaluated, leaving doubts on the strength of this method.

Recursive tracing

Shen et al [3] used size and position constraints for detecting the initial seed point on rib regions within binarized coronal image slices. They use edge detection approach to find the boundaries of the rib sections in the coronal image. This approach could lead to inaccurate segmentation results since most of the rib boundaries are ambiguous and not sharply defined, especially when the noise level is high. Nonetheless, they managed to limit the errors in the edges by using dynamic programming to join different boundary pieces and discard edges of nearby structures. The energy function to minimize was astutely constructed, including the distance between the two selected candidates on the *i* and *i+1* search direction, plus the correlation between two tangential vectors of these two points. Moreover, they careful designed the criterion for tracing validation at each step and the stopping condition to face the eventual deterioration of rib structure signals by noise, surrounding structures, and partial volume effect. In this work 40 multi-slice chest CT were tested, with a resolution in the range of 0.5~0.8mm in each direction. Patient profiles were not specified, hence assessments on the robustness of the method with respect patients conditions (gender, age, diseases) cannot be drawn. Furthermore, any kind of accuracy evaluation has been presented.


Fig. 14: Rib cross section contours

In a similar manner to Shen, also Zhang et al. [12] developed an algorithm that worked with coronal CT scans, but at each coronal slice rib regions were searched in the binarized image around the corresponding centroid point within a radius of 50pixels. They improved the rib detection process compared to Shen [3] by extracting at each coronal slice also the lung contours and increasing so the number of constraints on rib position. Additionally, they also included a further step to detect rib regions that were between the right and left lung contours when the slices contained spine regions. Although half of the CT data contained rib fractures, representing an optimal choice to test the algorithm performance, the size of the dataset was quite limited, counting only 15 images. Also in this study is not provided a proper quantitative evaluation of the segmentation results, but just some assessments from few radiologists who affirmed that the algorithm proved to work correctly, identifying ribs in 94.5% of the cases, and of the region extracted less than 1% was non-rib region. The segmentation of the complete set of rib structures from a dataset of 685 image slices took about 80 seconds.

The methods proposed from Shen and Zhang work on coronal slices, and not on planes perpendicular to the rib centerline, therefore in some frontal and rear slices the rib cross section will not be not anymore a small ellipse, but structures elongated along the horizontal direction, see fig. 15. In both studies, it is not specified if the methods corrected for those

areas, since there, given the changes of the rib cross section shapes, the stated constraints on rib's size and position are not expected to work anymore and could represent a limitation. A solution for this problem could be using planes perpendicular to the rib itself as Staal [6] and Yao [16] did, in such a way that the rib section shape remains a small ellipse. Another limitation of those methods is the high similarity of the clavicle's contours with the rib's contours on several coronal planes, which can cause the inclusion of the clavicles in the segmentation results. Moreover, difficulties with osteoporosis patients can be encountered when defining the seed points on the coronal slice, since the lower bone density associated with this disease makes the ribs signal fainter in the CT scan.

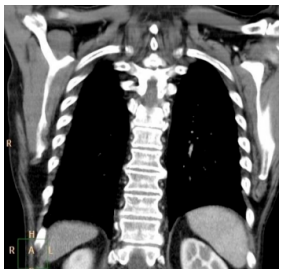

Fig. 15: Example of ribs elongated cross section.

H. Li et al. [10] tried to solve the mentioned problems by determining the seed points in a sagittal plane (the KSP). There, the ribs are emitted from the vertebrae to the sternum. Knowing that the ribs mineral density is higher close to the vertebrae than far from it, it is easier to obtain an expected contour of the ribs on the KSP than on coronal slices. Furthermore the clavicle shape is pretty different and therefore it can be easily distinguish from the ribs. However, as they focused only on the extraction of the center points of the rib sections, rib contours were poorly segmented, especially at the end of the ribs, in the connections with the sternum and vertebrae. The database used consisted of 21 CT images (11 males, 10 females, ages 18-90), with some patients presenting osteoporosis disease. The great efficiency time can be appreciated, with an average running time 4.95sec, on images composed by 104 slices on average. However, further effort in segmenting the rib boundary, together with an additional testing with clinical data, and a quantitative analysis of the obtained results, would be required to accept the method in clinical use.

Patient Info.		Image Info.				Results	
Sex	Age	*Slices*	*Resolution (xy/z) mm*	*Device Type*	*Efficiency*	*Positioning*	*Number of ribs*
M	64	120	0.78/3	T1	5s	correct	L12,R12
F	55	110	0.62/3	T2	4s	correct	L12,R12
M	18	111	0.67/3	T2	6s	correct	L12,R12
F	37	97	0.64/3	T3	5s	correct	L12,R12
M	55	168	0.54/3	T4	12s	correct	L12,R12
F	89	90	0.62/3	T2	4s	correct	L11,R11
M	90	90	0.68/3	T2	5s	correct	L11,R11
F	48	89	0.67/3	T1	4s	correct	L10,R10
F	74	105	0.75/3	T1	3s	correct	L12,R12
M	38	100	0.69/3	T2	5s	correct	L12,R12
M	24	115	0.72/3	T3	6s	correct	L12,R12
F	55	89	0.60/3	T3	5s	correct	L12,R12
F	82	86	0.61/3	T3	4s	correct	L11,R12
F	37	97	0.56/3	T4	5s	correct	L12,R12
M	75	125	0.78/3	T3	5s	correct	L12,R12
M	23	98	0.64/3	T3	4s	correct	L11,R11
M	63	100	0.72/3	T3	4s	correct	L11,R11
F	69	103	0.78/3	T3	5s	correct	L11,R11
M	35	95	0.71/3	T3	4s	correct	L11,R11
F	71	94	0.74/3	T3	4s	correct	L11,R11
M	54	94	0.69/3	T3	5s	correct	L12,R12

Table 3: Rib positioning and extraction results

The group of Yao et al. [14] achieved the ribs segmentation by using a progressive tracing technique that started with the segmentation of the spinal column. Using an algorithm previously developed by the same group and then refining the results with a vertebra template matching technique the segmentation of the vertebral column was obtained. In this way, the problem of similarity between rib sections and clavicle section encountered by Shen [3] and Zhang [12] was avoided. The ingenious intuition of extracting perpendicular rib cross section by searching for the plane that minimized the bony area present in the plane itself, instead of extracting other geometrical features, like Staal et al. [6] did with the Hessian matrix, allowed the algorithm to save important computational time. However, the method presented is only a part of Computed Aided Detection system, with the purpose of finding sclerotic bone metastasis in the ribs. Hence, the method has been tested and evaluated on 10 CT scans, without reporting the results of the segmentation framework. Further test and accurate performance evaluations are therefore required to make this method suitable for segmenting the whole rib cage, even if up to now it seems promising.

Region growing

The method of Fiebich et al. [7] grew the target volume iteratively, employing decreasing gray level thresholds and a maximum gradient value. In this way the segmentation results of an iteration were improved in the following iteration, preserving also the boundaries of the structures. This convincing approach relies on threshold values estimated from 3 CT scans. While this strategy could lead to erroneous parameters estimation, given the small number of data used, it avoids to overfit the parameters to the data, keeping the algorithm as general as possible. From the conducted experiments, this idea seems to be successful, since high performances are attained with quite different CT data, acquired from 4 different CT scanners (CTI and Advantage, GE Medical Systems, Milwaukee, WI,U.S.A.; SR7000 and Tomoscan LX, Philips Medical Systems, the Netherlands). However, precise conclusions on the effectiveness of those parameters can't be drawn, given the limited size of the database, and the absence of quantitative assessments of the results. Furthermore, whenever ribs' adjacent structures present very similar gray values, they are likely to be included in the segmentation, as for example when highly enhanced vessels are close to the bone, with partial volume effects obscuring the boundaries. Another limitation is that the ribs are segmented joined to the spine and the sternum, since there is no step that in the algorithm that provides such separation. To separate the ribs also here is suggested a rib cage model base approach like Klinder [5], that could extract from the final segmentation only the rib cage. The algorithm was evaluated on a total of 40 randomly chosen CT studies of three body parts, 20 studies of the head, 10 of the chest, and 10 of the abdomen. The computation time for the chest CT was on average 15sec, for an image composed of 100 slices. The results of the segmentation of the bony structures were only reviewed by two radiologists, which simply evaluated the grade of overlapping of the segmented structure with the original image. Both radiologists rated more than 86% of the images as good to excellent (perfect bone segmentation). The method is believed to provide reliable segmentation results, but it still need to be tested on a larger dataset with a well-grounded accuracy evaluation.

Kim et al.[8] proposed an interactive tracking method able to segment objects in consecutive slices of 3D images. The framework cannot be classified as automatic, as it requires user interventions in several occasions. While some physician would appreciate interfering with the segmentation process to improve the final result, it is often preferred a fast and automatic software, that allows to disburden doctors from analyzing the huge amount of data that the latest generation of CT-scanners are able to produce [6], [12]. Moreover if a rib fracture is present, doctors have to spend a lot of time to complete the rib fracture localization diagnosis [10]. In the present method, user given seed points were required both at the beginning of the region growing process to segment the vertebral column, and also at the end, to segment those ribs that in image slices appeared disconnected from the spine and therefore could not be segmented with propagation of the target object. Moreover, 10% of the images containing segmented vertebrae needed further investigation from an expert to improve the results, since severe leakage errors urged to be corrected. Finally the algorithm was tested on a poor data set of only 5 CT images. However, the author presented an appropriate quantitative evaluation, estimating the accuracy of the algorithm segmentation (improved from the expert) against a manual segmentation, with a result of 96% accuracy. Although it demonstrated to be a fairly efficient method, taking on average 70 sec per each CT data, the required user intervention could represent a time consuming step, often undesired in clinical setting. Furthermore, the segmentation results contain not only rib structures but also the spinal column and the others bones structure present in the thorax, therefore an additional step is mandatory to separate the ribs structures from the adjacent bone formations.

To solve the rib-spine separation problem faced by Fiebich [7], Lee et al [1] tried to use an expected distance between the seed detected and the vertebrae central line in the same fashion as Furuhashi [9]. However, also here, it wasn't specified how this "expected length" was determined. Deciding the correct distance between the detected seed point and the center of the vertebrae is a non-trivial process, especially if the expected distance is set for adult rib cages there could be difficulties when dealing with smaller size or pediatric rib cages. Finally, the algorithm was tested on a large dataset containing a total of 2632 ribs in 110 CT scans, of which an author estimated 2600 ribs to be correctly segmented (98.8%). The problematic ribs were the highest and lowest, for their short length they were segmented only in part or not at all. Although this method has been tested on such an extensive dataset, appearing powerful, it still has to be quantitative validated.
In the same manner of Lee et al. [1] and Furuhashi [9], Ramakrishnan et al. [13] used the distance from the detected spine centerline to know where to stop tracing the ribs centerline. Also in the work of Ramakrishnan's group, there was no explanation of how the expected distance was calculated. This method extracts robustly the ribs centerline after finding automatically ribs seed points on 3 coronal and 12 sagittal images among those bone regions that met rib size constraints. A downside of this method is that it allows seeds in non-rib bones, such as clavicles and scapula. The framework was evaluated on 149 CT images, containing contrast agent, metal screws in the sternum and in the spine and rib pathologies such as metastasis or fractures. The axial slice space ranged from 0.5 to 8.0mm, and the slice thickness varied from 1.0mm to 8mm. The axial resolution varied from 0.5 to 0.87mm. A total of 3069 ribs out of 3187 (96.29%) were successfully detected and traced to completion, within a computation time around 20sec per image. Given the dimension and the variety of the data set on which it was tested, and the results obtained, the only two missing element to classify the method as completely effective are a step to remove those seed points detected in clavicles and scapula, and a satisfying description (and evaluation) of the stop tracing criterions. This work could then successfully form the basis for the complete rib cage segmentation in a further step.

4.2. Prior knowledge based segmentation methods

Rib cage model based

To achieve an accurate initial position of the rib cage model Klinder et al [5] developed a ray search based procedure for the detection of the ribs positions in the CT volume. The data set used to build the model, does not contain any image of patients presenting severe rib cage deformities as scoliosis, or any kind of fractures (or at least is not specified). So the mean model only incorporates information of "healthy" rib cages. Moreover, a subset of the same data set for creating the model was used to test the method through the cross-validation technique, so the algorithm performances are unknown when applied to deformed rib cages. Unlike the majority of the studies, here the results evaluated quantitatively by calculating the distances between the automatically adapted rib cage model and its corrected version from the first author, which calculated the averaged mean and maximal values of the minimal, mean, maximal Euclidean distances between corresponding points, as shown in table 4. Automatic rib detection was successful in 16 cases out of 18, in one case the ray search based approach found just few rib candidates, so the rib centerline extraction failed and the model could not be positioned. Another case did not show a significant minimum after the model being registered. Hence, CT images with low resolution

and high noise level can represent a limitation of the present method, since there the ray search approach will not give precise results on the ribs midline extraction. However, the method is believed to perform robustly when few ribs are partially or completely missing, since then, the non matched-ribs will be positioned according to the adjacent (matched) ribs. This represents a huge advantage compared to the thresholding techniques, recursive tracing or region growing, that would stop the rib tracing in case a part of it is missing.

	vertebra adaptation			rib adaptation		
	min	mean	max	min	mean	max
d_{mean} [mm]	0.30	1.27	1.8	0.21	0.36	0.92
d_{max} [mm]	4.35	6.27	9.41	3.31	7.01	11.43

Table 4: Summary of model adaptation of 16 data sets

The computation time of this method is longer than the other method (~5min) and that might be an obstacle for a clinical usage. However, Klinder's group achieved a mean distance error over all data sets of 0.36 mm for the ribs, reaching a relevant level of accuracy on average.

Wu et al [11] developed an innovative hybrid method that employed a classifier to distinguish between rib bone voxels and non-rib bone voxels, refining the results with a template matching technique. To register the prior model to the new image Wu's group used a new kind of registration technique. Indeed, while rigid transformation does not suffice for rib cages registration, non-rigid transformations are computationally expensive and too vulnerable to local minimum. Therefore they shrewdly designed a segment to segment matching approach, that proved to be robust against local ambiguities or discontinuities. The database used was composed by 112 cases, showing a significantly variety of the size, shape and pathologies of the rib cage. Of those CT images, 40 were used for training the classification algorithm and 72 for testing the whole method. The method demonstrated to be also noticeably efficient taking only 40 seconds for extracting the centerlines of the whole ribcage. Such a positive performance has been achieved using a coarse to fine learning pyramid structure, but mostly because the use of a prior model avoided all those post processing steps as pairing and ordering. Moreover the method has been extensively evaluated, with also qualitative and quantitative comparisons against Ramakrishnan's method (indicated as 'Tracing' in table 6) and another method (RPM) that used a non-rigid registration technique [32]. The results are shown in table 5 and 6.

	RPM	Articulated Rigid Matching
pair 1	16.7	4.1
pair 2	12.4	1.5
pair 3-10	11.6	1.2
pair 11	11.2	1.6
pair 12	14.5	3.6

Table 6: average modified Hausdorff distances (mm) between the ground truth and the extracted centerlines

No. of Ribs	Tracing	Matching
Missed	138 (8.0%) /40 (55.6%)	0 / 0
False	55 (3.2%) /19 (26.4%)	0 / 0
Mislabeled	692 (40.0%) /46 (63.9%)	0 / 0

Table 5: Result error of two rib centerline extraction methods. Number of incorrect ribs/ number of volumes these incorrect ribs came from

Unfortunately, the presented work focuses only on the extraction of rib centerlines. However, for the results and efficiency achieved, and for the variety of the database on which it was tested, the method could definitely constitute the solid basis for a further complete segmentation of the all ribs.

Prior knowledge based

The group of Gargouri et al. [15] incorporated prior anatomical knowledge in their method by training a classifier (RF) to recognize rib-bone voxels to non-rib bone voxels. The training set employed was reasonably large, composed by 473,000 randomly chosen bone voxels (45% rib bones, 55% non rib bones) manually pre-labeled by an expert. Also the number of features used is considered to be abundant, since the class labels were only two (rib bone voxel, non rib-bone voxel). However, the features were obtained from male data, so it is not clear how the method will perform on female/child data. During the development of their two ingenious shape descriptors, the authors focused on make them robust with respect the patient position, and noise level, since as they also correctly claimed, homogeneous acquisition settings cannot be assumed when processing large databases of CT scans. The two new shape descriptors (AI and RISC) proved to be superior to the simple intensity based descriptor, especially with varied patient position, and with additive noise, see tables 7-9. Moreover, since the algorithm did not require any preregistration or smoothing step, it demonstrated to be extremely efficient, taking only 0.5 sec on average for the entire classification task. Such a descriptor seems therefore well suited for the automatic classification of rib bones in CT images, but further effort is required to separate accurately the ribs from adjacent bone structures. In fact, also in the image can be seen how rib voxel are sometime misclassified when overlap with the clavicle or in the proximity of sternum and spinal column.

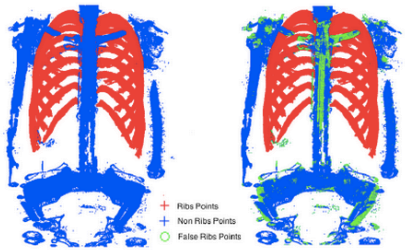

Fig. 16: Rib bone labeling: left, manual expert segmentation, right RF classification

	Baseline	AI	RISC
Correct classification	81.28%	87.22%	**97.33%**
False positives	3.02%	11.7%	1.01%

	Baseline	AI	RISC
Correct classification	92.12%	90.32%	**96.19%**
False positives	0.45%	7.54%	0.83%

Tables 8-8: Performance of RF classifier on a single CT scan using 3 shape descriptors in normal conditions (top table) and with the CT image rotated of 20°

	Baseline	AI	RISC
1% noise			
Correct classification	91.92%	87.51%	**96.92%**
False positives	2.18%	10.99%	0.81%
2% noise			
Correct classification	72.09%	76.38%	**97.48%**
False positives	24.42%	22.65%	0.68%

Table 7: Performance on the same CT scan but corrupted with additive noise

Staal et al. [6] achieved the segmentation of the complete rib cage with an approach that included primitives construction and classifications, followed by a seed growing technique. Cleverly, to create the primitives they did not only considered the gray values of the centerline neighbors but they took into account also their relative orientation with respect to the centerline. Since no information about patients profile included in the data set was presented in this study, the performance of the algorithm with contrast enhanced CT, as well as CT presenting fractures or severe ribs deformations is unknown. Difficulties could arise when CT scans present enhanced blood vessels, being also elongated structures with similar gray values, they could be included when detecting 1D ridge voxels, or be included as part of one rib, when they are in its close neighborhood. Fractures in the CT image are expected to decrease segmentation quality, since the algorithm might have problems in the first stage when determining the primitive in the fracture point, because there, the rib will not be anymore a single elongated structure. Moreover, if some ribs are partially or totally missing from the image, the algorithm will not be able to recover them, as instead could do model base techniques such as Wu [11] or Klinder [5]. An advantage of this method is that the features used for the classification process were astutely selected, using only the subset

of the total 72 features that gave the best classification results (24 features in their experiment). The database used consisted of 40 CT scans, 20 for the training step, and 20 for testing, with in-plane resolution varying between 0.57 mm and 0.91 mm. An extensive analysis of the results has been presented, reporting a quantitative assessment of the primitive classification, showing accuracy equal to 0.975, sensitivity of 0.968 and specificity of 0.978, see table 10. Furthermore, they conduced a qualitative, but detailed, evaluation of the full segmentation results, having no manual reference available. The results from the expert analysis are shown in table 11. It has to be said that they arbitrarily decided to ignore the first ribs both when defining the ground truth and in the test set, as they were not always visible. So further effort is required to completely segment also those first ribs. Moreover, in some cases the seeded region growing algorithm tends to over segment part of the ribs into the spine, not reflecting the truly length of those ribs. Another drawback of this method is the computational time estimated to be around 7 min for the whole process. The computation time could probably be reduced by using the idea of Yao et al. [14] to calculate the perpendicular rib cross sections, instead of calculating second derivatives in the Hessian matrix. Also if the Random Forest classifier had been developed earlier, probably the authors would have chosen for that, as Gargouri [15] did, given the high performances that it is capable to reach. One more limitation is that the misclassification of a single primitive is very costly since it leads to the inclusion or exclusion of a substantive structure. Given the great results achieved and the detailed assessment of the performance presented, if surmounted the few limitations reported, the method is considered to be adapt for usage in clinical setting.

		Reference		Total
		Rib	Non-rib	
Computer	Rib	3105 (31.0%)	147 (1.5%)	3252 (32.5%)
	Non-rib	103 (1.0%)	6661 (66.5%)	6764 (67.5%)
	Total	3208 (32.0%)	6808 (68.0%)	10016

Table 9: Confusion matrix for the primitive of the test set consisting of 20 scans with posterior probability thresholded at 0.85

	Into spine	Too short	Too long
Total	43	32	11
Average per scan	2.15	1.6	0.55
Percentage of detected ribs	9.9%	7.4%	2.5%

Table 10: Results of the qualitative evaluations of the rib segmentations

5. Conclusions

In the course of this literature review, diverse methods and ideas have been analyzed and evaluated. Each of the different methodologies presented strong and weak points, that made it more or less suitable for a usage in clinical setting.
A fundamental step, common in almost all of the methods considered, was binarizing with one or more specific threshold the CT volume, in order to show only the bony structures, while hiding the other structures like organs, cartilage, muscles etc. Hence, it's self-evident that the choice of the threshold value is a very critical and careful point [8]. Indeed, a slightly shifted threshold can have costly consequences, leading to the inclusion in the image of unwanted structures like contrast-enhanced vessels or calcified lesions or on the other hand to the exclusion of part of the bony structures. Therefore, further steps to eliminate the unwanted structures are always required.
The recursive tracing techniques are located half way between thresholding methods and seeded region growing methods [3]. First, using thresholding techniques, they detect a set of initial seed points on ribs on one image slice, then the ribs projections on that image slice are segmented and finally the segmentation is propagated in the following slices. However these methods have some difficulties. First, the noise in low dose CT data can be high, leading to obscure and broken rib boundaries. Second, the rib shapes vary considerably, making it hard to establish precise constraints. Finally, the other adjacent bone structures may digress the tracing paths.
Several works that employ region growing techniques to segment rib structures have been found. These methods segment the entire rib 3D volume by expanding an initial seed point with a set of constraints. They represent a valuable way of segmenting the rib cage but it is sometimes difficult to separate the ribs from the spine and sternum. Moreover, the constraints to use during the region growing have to be carefully evaluated, to not include unwanted structures in the segmentation result nor to leave out part of the ribs.
Model based segmentation is an innovative and promising technique that allows extracting objects with different shape from one image, given a priory general description of the object. It relies on a firm registration algorithm, capable of finding the target object in the image despite the inter-subject differences. Due to the prior shape constraints on the whole rib cage, model based techniques are considered to be robust and reliable, capable of segmenting the rib cage with acceptable results even when partial or total ribs are missing from the image. However, as also Klinder et al [5] state, these methods are strictly dependent on a good initialization of the model. Especially in the case of rib cages, with its amount of similar structures, once that the adaptation is misled it can hardly recover. Also, those methods can easily lead to results where the ribs in the detected rib cage are shifted with respect to the ground truth. This is due to the fact that the model will be locally well fitted to the data, and therefore cannot escape from such a local minimum [6]. Furthermore, can be notice how those techniques are highly insensitive to deforming bone pathologies or fractures, imposing the prior model over the new CT volume they frequently do not allow for such fine deformations.
The present literature study proposed an exhaustive overview of the techniques used for rib cage segmentation in CT scans, aiming to provide a complete understanding of the topic and the related difficulties, fundamental for future improvements in this field.

6. References

[1] * Jaesung Lee and Anthony P. Reeves: "Segmentation of Individual Ribs from Low-dose Chest CT" Medical Imaging 2010: Computer-Aided Diagnosis, Proc. of SPIE Vol. 7624 76243J-1 (2010)

[2] * Shantanu Banik, Rangaraj M. Rangayyan, and Graham S. Boag: "Automatic Segmentation of the Ribs, the Vertebral Column, and the Spinal Canal in Pediatric Computed Tomographic Images" Journal of Digital Imaging, Vol 23, No 3, 301–322 (2010)

[3] * H. Shen, L. Liang2, M. Shao, and S. Qing: "Tracing Based Segmentation for the Labeling of Individual Rib Structures in Chest CT Volume Data" : MICCAI 2004, LNCS 3217, pp. 967–974, (2004)

[4] * X. Zhou, T. Hayashi, M. Han, H. Chen, T. Hara, H. Fujita, R. Yokoyama, M. Kanematsu and H. Hoshi "Automated Segmentation and Recognition of the Bone Structurein non-Contrast Torso CT Images using Implicit Anatomical Knowledge" Medical Imaging, Proc. of SPIE Vol. 7259 72593S-1 (2009)

[5] * T. Klinder, C. Lorenz, J. von Berg, S. P.M. Dries, T. Bulow, and J. Ostermann "Automated Model-Based Rib Cage Segmentation and Labeling in CT Images" MICCAI, Part II, LNCS 4792, pp. 195–202, (2007)

[6] * Joes Staal, Bram van Ginneken *, Max A. Viergever :"Automatic rib segmentation and labeling in computed tomography scans using a general framework for detection, recognition and segmentation of objects in volumetric data" ELSEVIER Medical Image Analysis 11, 35–46 (2007)

[7] * Fiebich, Martin; Straus, Christopher M.; Sehgal, Vivek; Renger, Bernhard C.; Doi, Kunio; Hoffmann, Kenneth R.: "Automatic Bone Segmentation Technique for CT Angiographic Studies" Journal of Computer Assisted Tomography, Volume 23(1) pp 155-161, January/February (1999)

[8] * D. Kim, H. Kim, H. Sik Kang: "An Object tracking segmentation method: vertebra and rib segmentation in CT images" From Conference Volume 4684, Medical Imaging 2002: Image Processing, Milan Sonka; J. Michael Fitzpatrick, San Diego, CA | February 23 (2002)

[9] * S. Furuhashi, K. Abe1 M. Takahashi, T. Aizawa, T. Shizukuishi, M. Sakaguchi, T. Maebayashi, I. Tanaka, M. Narata, Y. Sasaki: "A Computer-Assisted System for Diagnostic Workstations: Automated Bone Labeling for CT Images" Journal of Digital Imaging, Vol 22, No 6 : pp 689-695 (December), (2009)

[10] * Hong Li; Shenyang; Jun Li ; Shinong Pan ; Qiyong Guo: "Automatic Rib Positioning Method in CT Images" 4th International Conference on Bioinformatics and Biomedical Engineering (iCBBE) pp 1 – 4 18-20 June (2010)

[11] * D. Wu, D. Liu, Z. Puskas, C. Lu, A. Wimmer, C. Tietjen, Grzegorz, Soza, and S. K. Zhou "A learning based deformable template matching method for automatic rib centerline extraction and labeling in CT images" IEEE Conference on Computer Vision and Pattern Recognition (CVPR), pp 980 – 987 16-21 June (2012)

[12] * Li Zhang, Xiaodong Li, Qingmao Hu "Automatic Rib Segmentation in Chest CT Volume Data" Proceedings of the 2012 International Conference on Biomedical Engineering and Biotechnology (ICBEB) pp 750-753 (2012)

[13] * S. Ramakrishnan, C. Alvino, L. Grady, A. Kiraly: "Automatic three-dimensional rib centerline extraction from CT scans for enhanced visualization and anatomical context" Conference Volume 7962 Medical Imaging 2011: Image Processing, February 12, (2011)

[14] * Jianhua Yao, Burns J.E., Summers R.M.: "Sclerotic rib metastases detection on routine CT images" IEEE International Symposium on Biomedical Imaging (ISBI) pp. 1767–1770, 2–5 May (2012)

[15] * M. Gargouri, J. Tierny, E. Jolivet, P. Petit : "Accurate and robust shape descriptors for the identification of RIB cage structures in CT-images with Random Forests" 10th International Symposium on Biomedical Imaging (ISBI), IEEE pp 65-68 7-11 April (2013)

[16] J. Yao, S. D. O'Connor, and R. M. Summers, "Automated Spinal Column Extraction and Partitioning," presented at IEEE ISBI, Arlington, VA, (2006)

[17] D. Mitton, K. Zhao, S. Bertrand, C. Zhao, S. Laporte, C. Yang, K.-N. An, W. Skalli: "3D reconstruction of the ribs from lateral and frontal X-rays in comparison to 3D CT-scan reconstruction", Journal of Biomechanics 41, 706–710 (2008)

[18] M.L. Giger, K. Doi, and H. MacMahon, C.E. Metz, F. F. Yin: "Pulmonary Nodules: Computer Aided Detection in Digital Chest Images" Radiographics 10, 41–51 (1990)

[19] H. Yoshimura, M.L. Giger, K. Doi, and H. MacMahon, S. Montner : " Analysis of Computer Reported False-Positive Detections of Lung Nodules in Digital Chest Radiography" Med. Phys. 17, 524 (P) (1990)

[20] Peter De Souza: "Automatic Rib Detection in Chest Radiographs" Computer Vision, Graphics and Image Processing 23, 129-161 (1983)

[21] S. Sanada, K. Doi, H. MacMahon: "Image future analysis and computer aided diagnosis in digital radiography: Automated Delineation of Posterior Ribs in Chest Images" Med. Phys. 18 (5), 964–971 (1991)

[22] Z.Yue, A.Goshtabsy, L.V. Ackerman "Automatic Detection of Rib Borders in Chest Radiographs" IEEE Transition on medical imaging, vol. 14, n 3 (1995)

[23] Volgelsang, F., Weiler, F., Dahmen, J., Kilbinger M., Wein, B., Gunther, R.W., "Detection and compensation of rib structures in chest radiographs for diagnose assistance" Proceedings of SPIE, 3338:774-785, (1998)

[24] R. Moreira, A. M. Mendonc , and A. Campilho: "Detection of Rib Borders on X-ray Chest Radiographs" ICIAR, LNCS 3212, pp. 108–115, (2004)

[25] Ean Dansereau and Ian A. F. Srokest :"Measurements of the Three-Dimensional Shape of the Rib Cage" J. Biomechanics. 21. No. II, pp. 893–401 (1988)

[26] Said Benameur*, Max Mignotte, François Destrempes, and Jacques A. De Guise : "Three-Dimensional Biplanar Reconstruction of Scoliotic Rib Cage Using the Estimation of a Mixture of Probabilistic Prior Models" IEEE TRANSACTIONS ON BIOMEDICAL ENGINEERING, VOL. 52, NO. 10, OCTOBER (2005)

[27] Christopher, Koehler, Thomas, Wischgoll: "Knowledge Assisted 3D Reconstruction and Visualization of Human Ribcage and Lungs" IEEE Computer Graphics and Applications, (2009)

[28] E. Jolivet, B. Sandoz, S. Laporte, D. Mitton, W. Skalli: "Fast 3D Reconstruction of the Rib Cage from Biplanar Radiographs" Med Biol Eng Comput 48:821–828 (2010)

[29] J. Dworzak, H. Lamecker, J. von Berg, T. Klinder, C. Lorenz, D. Kainmüller, H. Seim, H.C. Hege, S. Zachow "3D Reconstruction of the Human Rib Cage from 2D Projection Images using a Statistical Shape Model" Int J CARS ,5:111–124 (2010)

[30] Lama Seoud, Farida Cheriet, Hubert Labele, and Jean Dansereau: "A Novel Method for the 3-D Reconstruction of Scoliotic Ribs From Frontal and Lateral Radiographs" IEEE TRANSACTIONS ON BIOMEDICAL ENGINEERING, VOL. 58, NO. 5, MAY (2011)

[31] Sébastien Grenier, Stefan Parent, Farida Cheriet: "Personalized 3D reconstruction of the rib cage for clinical assessment of trunk deformities" ELSEVIER Medical Engineering & Physics (2013)

[32] H. Chui, A. Rangarajan: "A new point matching algorithm for non-grid registration" Comput Vis Image Und, 89 (2-3), pp 114-141 (2003)